Chemistry of ion coordination and hydration revealed by a K^+ channel–Fab complex at 2.0 Å resolution

Yufeng Zhou, João H. Morais-Cabral*, Amelia Kaufman & Roderick MacKinnon

Howard Hughes Medical Institute, Laboratory of Molecular Neurobiology and Biophysics, Rockefeller University, 1230 York Avenue, New York, New York 10021, USA

Ion transport proteins must remove an ion's hydration shell to coordinate the ion selectively on the basis of its size and charge. To discover how the K^+ channel solves this fundamental aspect of ion conduction, we solved the structure of the KcsA K^+ channel in complex with a monoclonal Fab antibody fragment at 2.0 Å resolution. Here we show how the K^+ channel displaces water molecules around an ion at its extracellular entryway, and how it holds a K^+ ion in a square antiprism of water molecules in a cavity near its intracellular entryway. Carbonyl oxygen atoms within the selectivity filter form a very similar square antiprism around each K^+ binding site, as if to mimic the waters of hydration. The selectivity filter changes its ion coordination structure in low K^+ solutions. This structural change is crucial to the operation of the selectivity filter in the cellular context, where the K^+ ion concentration near the selectivity filter varies in response to channel gating.

Potassium channels control the electric potential across cell membranes by catalysing the rapid, selective diffusion of K^+ ions down their electrochemical gradient[1]. The structure of the K^+ channel has provided a firm basis for understanding the mechanisms of rapid K^+ ion transport underlying electrical signalling in cells[2]. Through the interactions of dehydrated K^+ ions within the channel's selectivity filter, high conduction rates are achieved in the setting of exquisite ion selectivity[3]. Two fundamental questions surrounding this process are addressed in the present study. The first is how the K^+ channel mediates the transfer of a K^+ ion from its hydrated state in solution to its dehydrated state in the selectivity filter. The issue of dehydration is relevant to all mechanisms of selective ion transport, and because dehydration in the wrong environment is energetically costly, we should expect to discover in the K^+ channel a very precise set of mechanisms designed to handle hydrated K^+ ions, and to mediate their dehydration.

The second question addressed in this study is related to the cellular environment in which K^+ channels operate: inside the cell the K^+ concentration is greater than 100 mM, whereas on the outside the K^+ concentration is usually less than 5 mM. The K^+ channel gate, or door that opens and closes the pore, is located between the selectivity filter and the intracellular solution[2,4–6]. Therefore, when the gate is open, the filter is exposed to a high K^+ concentration from inside the cell, and when it is closed the filter is exposed to a low K^+ concentration from outside. This is an interesting situation when one considers the structure of the selectivity filter, and the mechanism by which it conducts K^+ ions. The filter points a large number of carbonyl oxygen atoms into the pore. Owing to the partial negative charge on these atoms, this would be an unlikely structure if it were not for the presence of dehydrated K^+ ions in the filter. In other words, the K^+ ions that go through the filter are actually counter-charges, necessary for its structure. The question that then arises is what happens when the channel's gate closes and the selectivity filter is in equilibrium with a low extracellular K^+ environment. We answer this by describing the structure of the K^+ selectivity filter in the presence of a low K^+ ion concentration.

K^+ channel–Fab complex

To address the above questions it was necessary to solve the K^+ channel structure at a resolution that would reveal ordered water molecules and protein chemistry with high accuracy. To achieve this end, we raised monoclonal antibodies against the KcsA K^+ channel and selected clones on the basis of their ability to recognize the tetrameric but not the monomeric form of the channel[7,8]. A K^+ channel–Fab complex with a stoichiometry of one Fab fragment per channel subunit was produced and crystallized in space group *I*4, with one channel subunit and Fab fragment per asymmetric unit. Frozen crystals diffracted X-rays to 2.0 Å Bragg spacings at the synchrotron. We solved phases by molecular replacement using a published Fab structure (Protein Data Bank (PDB) code 1MLC)[9], and could easily interpret the resulting electron density map. The published KcsA K^+ channel structure (PDB code 1BL8) was placed into the density map[2], followed by several cycles of rebuilding and refinement. The final model, referred to as the high-K^+ structure (200 mM K^+), is refined with good stereochemistry to an R_f and R_w of 23.3% and 21.8%, respectively, and contains 534 amino acids, 7 K^+ ions, 469 water molecules and 2 partial lipids. A second structure, the low-K^+ structure (3 mM K^+), was solved at 2.3 Å resolution to an R_f and R_w of 23.5% and 21.8%, respectively, and contains 534 amino acids, 2 K^+ ions, 1 Na^+ ion, 266 water molecules and 2 partial lipids (Table 1).

The Fab fragment is attached to the K^+ channel turret on the extracellular face of the channel (Fig. 1). All of the protein contacts within the crystal are formed between neighbouring Fab fragments, with the K^+ channel conveniently suspended so that its detergent micelle is not involved in crystal contacts. This packing arrangement undoubtedly accounts for the high-quality X-ray diffraction[7,8]. Furthermore, Fab attachment to the turrets leaves open a wide passageway outside the pore, so that ion binding should be unperturbed by the presence of the Fab fragments.

An electron density map surrounding the channel's selectivity filter in the high K^+ structure is shown in Fig. 2. Density is present at four K^+ ion-binding sites inside the selectivity filter, corresponding to positions 1–4 from outside the cell to inside. Strong electron

* Present address: Department of Molecular Biophysics and Biochemistry, Yale University, 260 Whitney Avenue, New Haven, Connecticut 06520, USA.

Table 1 Crystallographic analysis

Data set	Data collected					
	Resolution (Å)	Redundancy, overall/outer	Completeness, overall/outer (%)	R_{symm}*, overall/outer	I/σ, overall/outer	Reflections with $I/\sigma > 2$, overall/outer (%)
High K^+	50–2.0	3.8/3.0	99.1/95.2	0.071/0.530	22.4/2.3	79/45
Low K^+	30–2.3	4.2/2.7	99.2/95.3	0.056/0.370	24.5/2.2	80/40

	Refinement			Root mean square difference		
	Resolution (Å)	R_w/R_f† (%)	Mean *B*-factor (Å^2)	Bond lengths (Å)	Bond angles (°)	*B*-factor (Å^2)
High K^+	40–2.0	21.8/23.3	37.4	0.007	1.4	0.7
Low' K^+	30–2.3	21.8/23.5	49.2	0.007	1.4	0.7

*$R_{symm} = \Sigma\Sigma|\langle I\rangle - I_i| / \Sigma\langle I\rangle$
†$R_w = \Sigma||F_o| - |F_c|| / \Sigma|F_o|$. R_f is defined as R_w calculated with 10% of reflections excluded from the refinement.

density is also visible at both entryways to the filter, curiously suspended along the pore axis.

K^+ hydration in the central cavity

A unique feature of the K^+ channel structure is that its ion conduction pore dilates to about 10 Å diameter at one point. The dilation, called the central cavity, occurs at the intracellular side of the selectivity filter, halfway across the membrane (Fig. 1b). The presence of the cavity can be understood intuitively as one of the channel's mechanisms for overcoming the dielectric barrier, or repulsion by the low-dielectric membrane, by keeping the K^+ ion in a watery, high-dielectric environment[2,10]. The electron density at the intracellular entryway to the selectivity filter corresponds to a K^+ ion at the centre of the cavity (Fig. 2, bottom density). Remarkably, this ion is fully hydrated by eight discrete water molecules, four 'above' and four 'below' the K^+ ion (Fig. 3). The appearance of water density in the cavity is influenced by the ionic species and by adding inhibitors that bind in the cavity (not shown). These observations ensure that the density surrounding K^+ in the cavity represents ordered water molecules and not a build-up of noise due to crystallographic symmetry. This structure, a K^+ hydration complex, is suspended at the cavity centre, too far from the cavity walls to make direct contact with protein atoms. There is ample space for additional water molecules in the cavity, but they are disordered: only the water molecules in the inner hydration shell of the K^+ ion are sufficiently ordered to be visible in the X-ray structure at the contour shown.

The absence of visible water molecules at the surface of the cavity is as significant as the presence of water around the K^+ ion. The cavity in KcsA and most other K^+ channels is lined mainly by hydrophobic amino acids from the inner helix (Ile 100, Phe 103; Fig. 3) that do not provide strong hydrogen-bonding donor or acceptor groups. Consequently, water in the cavity is available to interact strongly with the K^+ ion without competition from the protein surface. That said, the compelling question arises of why the water molecules around the K^+ ion are so precisely ordered, rather than being spread evenly over a spherical shell. Inspection of the cavity wall shows that the order is probably imposed by a sum of very weak, indirect hydrogen-bonding interactions mediated by certain chemical groups, such as the hydroxyl group of Thr 107, and perhaps the carbonyl oxygen atoms from the pore and inner helices. In support of this idea, electron density maps at lower contours show a less ordered water molecule acting as a bridge connecting the Thr 107 hydroxyl group to the K^+ hydration complex (not shown). The probable significance of a geometric match between the cavity and a K^+ ion is implied by the absence of a complete shell of visible water molecules when Na^+ rather than K^+ is in the cavity. Thus, a K^+ hydration complex is held in a surprisingly precise configuration at the centre of the cavity. The four-fold distribution of water molecules surrounding the K^+ ion causes one to wonder whether the fundamental structure of a hydrated K^+ ion gave rise to a four-fold symmetric channel.

Visualization of an organized K^+ hydration complex brings our understanding of the K^+ channel cavity to a deeper level. Continuum electrostatic calculations showed that a high-dielectric (water-filled) environment and oriented pore α-helices (KcsA

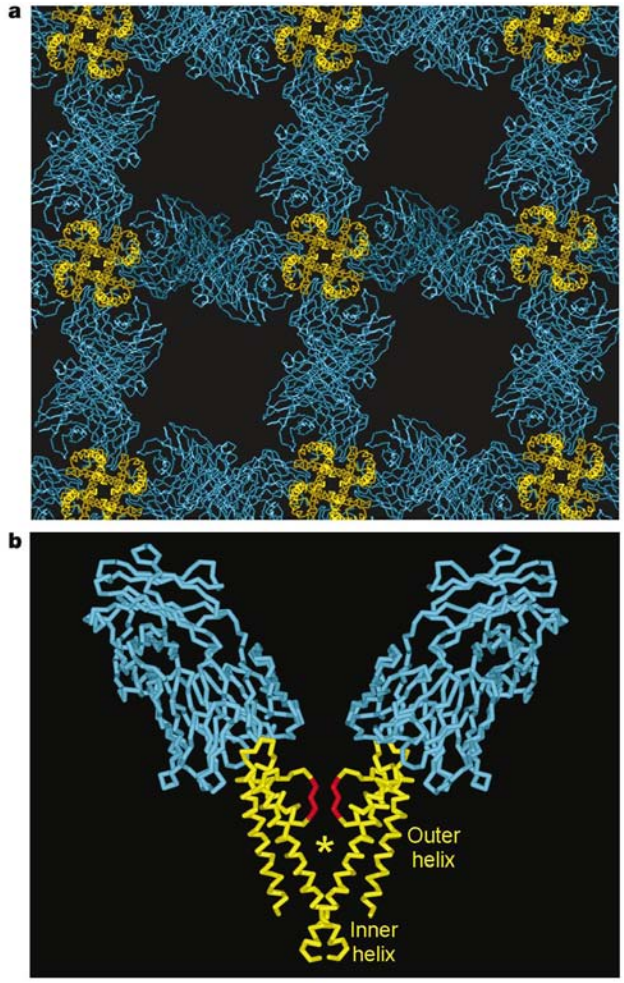

Figure 1 Fab attachment and crystal packing. KcsA (yellow) was crystallized as a complex with an antibody Fab fragment (blue). One Fab fragment is bound to the extracellular-facing turret on each K^+ channel subunit. **a**, View down the four-fold crystallographic axis of the *I*4 cell, which corresponds to the molecular four-fold axis of the K^+ channel. **b**, Two subunits and attached Fab fragments viewed perpendicular to the four-fold axis. The transmembrane outer and inner helices are labelled. The asterisk denotes the location of the central cavity, below the selectivity filter (red).

residues 61–73) account for K^+ ion stabilization in the cavity[10]. However, these electrostatic considerations predict a relatively broad energy minimum; they do not account for the very focal nature of the ion observed in electron density maps. Localization of the K^+ ion at the cavity centre is now explained by the water structure around the ion: because the cavity holds the ion and its surrounding water molecules, the ion stays at the centre. But the ordering of water molecules should in no way impede the movement of a K^+ ion through the pore, because the exchange of crystallographically ordered water molecules can occur in less than a nanosecond timescale, whereas conduction occurs on the nanosecond timescale[11]. Through its design, the cavity ultimately achieves a very high effective K^+ concentration (~2 M) at the centre of the membrane, with the K^+ ion positioned on the pore axis, ready to enter into the selectivity filter.

K^+ dehydration at the extracellular entryway

The selectivity filter opens directly to the extracellular solution in such a manner as to expose four carbonyl oxygen atoms from the Gly 79 residues (Fig. 4a). These carbonyls are directed straight out into solution in a ring surrounding the perimeter of the pore entryway. Buried just beneath the protein surface, carboxyl-carboxylate pairs formed by the side chains of Glu 71 and Asp 80 provide four negative charges near the entryway (Fig. 2)[12]. Thus, the extracellular pore entryway is quite electronegative and should be attractive to a cation. Electron density maps show a complex structure close to the pore entryway consisting of two strong peaks on the pore axis associated with weaker surrounding density (Fig. 4a). For electrostatic reasons it is unlikely that these two peaks represent two K^+ ions coexisting at the pore entryway. By replacing Cl^- with electron-dense I^- in the crystals, we excluded the possibility that one of the peaks is related to a K^+ counter ion (not shown). We propose that the two on-axis peaks represent alternate positions of a single K^+ ion. The alternate positions are entirely consistent with our description of the K^+ conduction mechanism, in which the selectivity filter exists mainly in two ion configurations, K^+-water-K^+-water (1,3 configuration) and water-K^+-water-K^+ (2,4 configuration) (Fig. 4b)[3]. Through electrostatic interactions between an ion at the entryway and ions within the selectivity filter, the occurrence of the 1,3 and 2,4 configurations should result in displacement of the entryway ion, yielding two peaks of electron density. When the entryway ion is furthest from the pore (associated with the 1,3 configuration), it must be fully hydrated, but when it moves into its position near the pore (associated with the 2,4 configuration), the carbonyl oxygen atoms from the four Gly 79 residues are close enough to displace half of the ion's hydration shell. We interpret the electron density surrounding the two on-axis peaks as a superposition of water molecules associated with the entryway K^+ ion in its two positions. It is evident that the role of the Gly 79 carbonyl oxygen atoms, pointing straight into solution, is to assist in the hydration and dehydration of a K^+ ion at the extracellular entryway.

Two filter structures under high and low K^+ concentrations

The high-resolution structure of the selectivity filter in the presence of 200 mM K^+ is shown in Fig. 5a. The K^+ ions in positions 1–4 represent the average superposition of K^+ in the 1,3 and 2,4 configurations[3]. The arrangement of eight oxygen atoms surrounding each K^+ ion in the selectivity filter resembles the arrangement of water oxygen atoms around K^+ in the cavity (Figs 3 and 5a). In each case, K^+ resides near the centre of a distorted cube—a square antiprism—in which the square plane of oxygen atoms 'above' the ion is rotated with respect to the plane 'below'. In the filter, the oxygen–K^+ coordination distances range from 2.70 to 3.08 Å, with a

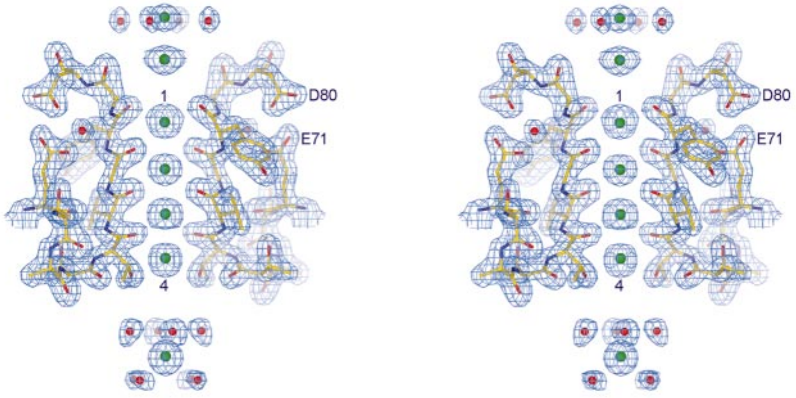

Figure 2 Stereo view of electron density in the region of the K^+ channel selectivity filter. The $2F_o - F_c$ electron density map (contoured at 2σ) covers amino acids forming the selectivity filter (two diagonally opposed subunits are shown), with K^+ ions (green spheres) along the ion pathway, and water molecules (red spheres) in the vicinity.

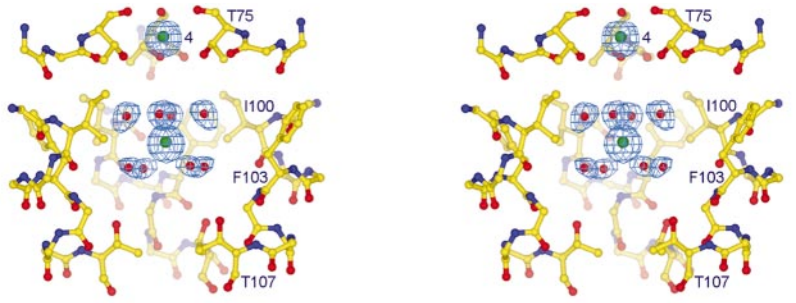

Figure 3 Stereo view of a hydrated K^+ ion in the central cavity. Eight water molecules (red spheres) surround a single K^+ ion (green sphere) in the cavity. The $2F_o - F_c$ electron density map is contoured at 2σ. Residues forming the cavity are shown in ball-and-stick representation. For clarity, only backbone atoms and the side chains facing the cavity (Thr 75, Ile 100, Phe 103, Gly 104 and Thr 107) are shown. The subunit closest to the viewer has been removed.

mean value of 2.85 Å. The distances are very similar to those observed in the K^+-selective antibiotics nonactin (2.73–2.88 Å) and valinomycin (2.74–2.85 Å)[13–15]. The selectivity filter is stabilized by a network of hydrogen bonds to the amide nitrogen atoms that point away from the pore, into the protein core. The network includes a short hydrogen bond (2.65 Å) between the carboxylic group of Glu 71 and that of Asp 80 (a carboxyl-carboxylate), and a buried water molecule bonded to the amide nitrogen of Gly 79 (ref. 12). The atomic temperature factors in this region of the protein are low (15–20 $Å^2$, compared with 37 $Å^2$ overall), indicating that the filter has a fixed, well defined structure, as expected for a high-throughput catalytic device[16]. Certainly the filter has to adjust its structure as ions move between the 1,3 and 2,4 ion configurations[3]. But refinement of the two configurations indicates that the structural adjustments are very small (not shown).

The low-K^+ structure of the selectivity filter (3 mM K^+) is significantly different than the high-K^+ structure (200 mM K^+) (Fig. 5b and c). In particular, ions are absent at positions 2 and 3 and the Val 76 and Gly 77 residues have adopted completely new conformations. The Val 76 carbonyl, instead of pointing toward the pore to coordinate a K^+ ion, is hydrogen bonded to a water molecule outside the pore, which in turn is hydrogen bonded to the amide nitrogen of Gly 77 on an adjacent subunit. The α-carbon of Gly 77 is twisted inward and occludes the pore, giving the filter an hourglass appearance. The hydrogen bond network is reorganized and a belt of buried water molecules now surrounds the perimeter of the selectivity filter inside the protein core.

This low-K^+ structure undoubtedly represents a non-conductive state of the selectivity filter, because it is essentially pinched shut. Given the large conformational differences between the high- and low-K^+ structures, it is likely that their rate of interconversion occurs more on the timescale of gating (milliseconds) than that of ion conduction (nanoseconds). The low-K^+ structure underlies the electron density profiles in low concentrations of K^+ and Rb^+ in an accompanying paper[3], where electron density peaks for ions were observed in positions 1 and 4, with a weaker peak presumably due to a water molecule at position 3. We propose that the K^+ channel begins to conduct ions only once the filter snaps into a main chain conformation similar to that observed in the high-K^+ structure (Fig. 5a). The discovery of two distinct structures under different ionic conditions does not imply that the selectivity filter is poorly structured, but rather that it can adopt two unique conformations driven by the K^+ concentration. Certainly, in high-K^+ ion concentrations under which conduction occurs, the structure of the filter is quite inflexible.

The low-K^+ structure explains how the selectivity filter maintains its stability in a low-K^+ environment; a dehydrated K^+ ion is lost but compensatory structural changes occur. These structural changes would have to be very important in a cellular environment, because the activation gate in K^+ channels, formed by the inner helices, is located between the selectivity filter and the cytoplasm (Fig. 1)[2,4–6]. This arrangement means that when the activation gate is open the filter 'sees' the high cellular K^+ concentration (>100 mM) and when it is closed the filter 'sees' the extracellular solution (<5 mM) (Fig. 6). The selectivity filter presumably responds by switching between the high- and low-K^+ structures when the channel gates.

We do not mean to imply that the selectivity filter is the activation gate. The design of a K^+ channel is such that the filter, on the extracellular side of the pore, serves the task of selective ion conduction, whereas the activation gate, on the intracellular side, opens and closes the pore. Although these functions are separate, the activation gate and the filter can obviously be coupled. One mechanism of coupling is through the K^+ gradient across the cell membrane, as described (Figs 5 and 6), and another potential mechanism is through direct structural perturbations propagated through the protein. By either mechanism, the high- and low-K^+ structures offer a physical explanation for phenomena that electro-

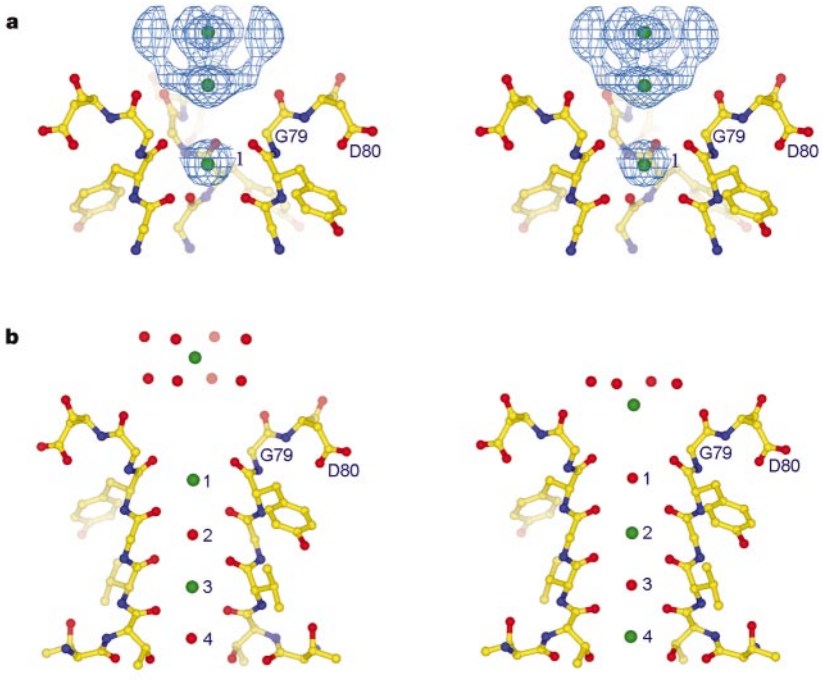

Figure 4 Potassium ion dehydration at the extracellular pore entryway. **a**, Stereo view of electron density ($2F_o - F_c$, contoured at 1σ) at the extracellular pore entryway. Channel amino acids are shown in ball-and-stick representation (with the subunit closest to the viewer removed) and K^+ ions as green spheres. Density for the K^+ ion at selectivity filter position 1 is shown for reference. **b**, Interpretation of the two ion peaks outside the selectivity filter. When the configuration of ions (green spheres) and water (red spheres) inside the filter is K^+-water-K^+-water (left; 1,3 configuration), an ion at the entryway is displaced further away. When the configuration is water-K^+-water-K^+ (right; 2,4 configuration), the ion outside the filter is drawn closer to the pore. The electron density outside the filter is proposed to be the average superposition of these ion positions with their associated water molecules.

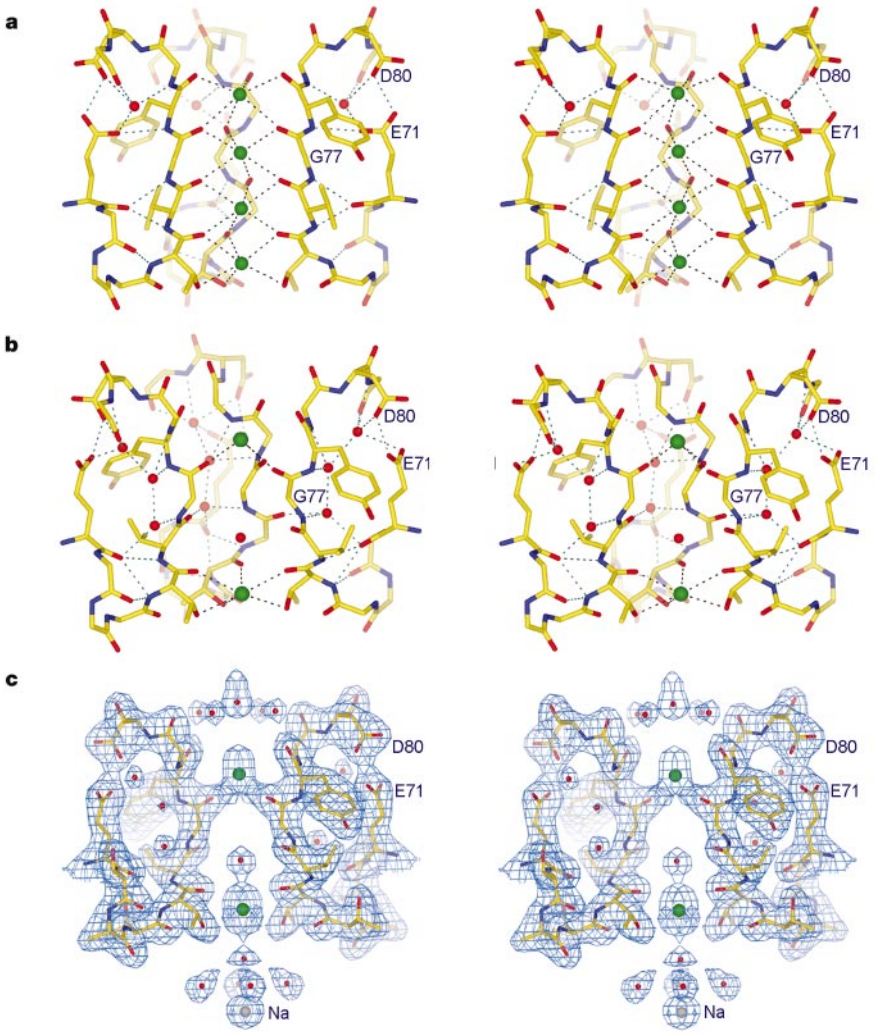

Figure 5 High- and low-K^+ structures of the selectivity filter (stereo views). **a**, The high-K^+ structure with K^+ ions (green spheres) in filter positions 1–4 (top to bottom). Each K^+ ion is located at the centre of eight oxygen atoms. The distances between the K^+ ions and the oxygen atoms (black dashed lines) above/below are: position 1, 2.80/3.08 Å; position 2, 2.72/2.83 Å; position 3, 2.85/2.70 Å; position 4, 2.94/2.88 Å. Important hydrogen bonds (blue dashed lines) and a buried water molecule (red sphere) are shown. For clarity, the subunit closest to the viewer has been removed and side chains of the following residues are not shown: Thr 72, Ala 73, Thr 74 and Leu 81 of all three subunits, and Val 76 and Tyr 78 from the subunit at the back. **b**, The low-K^+ structure. Atoms are represented as in **a**. **c**, Electron density map ($2F_o - F_c$, 1.5σ) validating the low-K^+ structure. Density at the centre of the cavity below the filter is modelled as Na^+ (silver sphere), the predominant cation present in the crystallization solution.

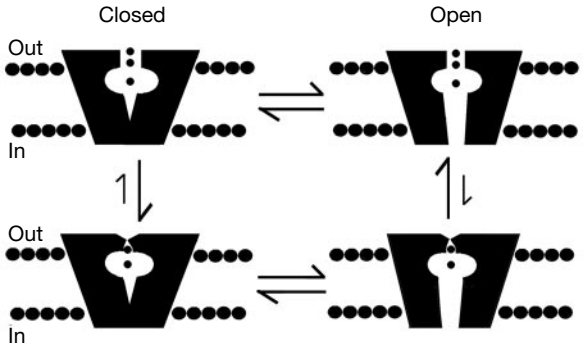

Figure 6 Biological significance of the K^+-dependent structural change in the selectivity filter. The K^+ ion gradient across the cell membrane (high K^+ inside, low K^+ outside) causes the K^+ concentration at the selectivity filter to vary as the activation gate (near the intracellular pore opening) opens and closes. The scheme implies that when the gate is closed the filter should adopt the low-K^+ structure (lower left), and when the gate opens and K^+ flows out the filter should adopt its high-K^+ structure (upper right). Transitions between the low- and high-K^+ structures in the setting of an open activation gate (upper and lower, right) should appear as gating in single channel records.

physiologists have long referred to as permeant ion effects on gating[17–19].

The two filter structures also may explain apparent gating transitions that seem to occur by mechanisms other than opening and closing the activation gate. For example, in Shaker K^+ channels, which have a voltage-dependent activation gate, brief, voltage-independent closures of the open channel are observed and are sensitive to mutations near the selectivity filter[20–22]. Such closures may represent millisecond-timescale fluctuations back and forth between the two conformations of the selectivity filter, as depicted by the two channels on the right side of Fig. 6. We propose that the underlying explanation for apparent gating of the selectivity filter, and for many of the permeant ion effects on gating, is that the selectivity filter has the capability of adopting two structures, one that conducts ions and one that does not. The ability to adopt two structures stems from the basic requirement of the filter to have an inbuilt mechanism for adjusting to the high- and low-K^+ concentrations that result from channel gating.

Summary

High-resolution structure determination of a K^+ channel–Fab

complex has allowed us to address the mechanisms of K^+ ion hydration and dehydration, and the response of the selectivity filter to the changing ionic environment imposed by channel gating. Three new principles of K^+ channel function are described. First, the central cavity holds a K^+ ion surrounded by eight ordered water molecules. The unique picture of a hydrated K^+ ion results from a geometric and chemical match between the cavity and the K^+ hydration complex. The cavity achieves a very high effective K^+ concentration (~2 M) at the membrane centre, with a K^+ ion positioned on the pore axis, ready to enter the selectivity filter. Second, the transfer of a K^+ ion between the extracellular solution (where a K^+ ion is hydrated) and the selectivity filter (where the ion is dehydrated) is mediated by a specific arrangement of carbonyl oxygen atoms that protrude into solution. A K^+ ion at the filter threshold senses the electrostatic field due to the ion distribution within the filter, and is drawn from a fully hydrated position to a position where it is half hydrated. Third, the selectivity filter can exist in two distinct conformations and the K^+ ion concentration drives the equilibrium between them. At a K^+ concentration of a few millimolar, the filter loses one of its dehydrated K^+ ions and undergoes compensatory structural changes that render it non-conductive. At higher K^+ concentrations the filter adopts a structure compatible with ion conduction. These conformational changes are crucial to the operation of the selectivity filter in the cellular context, where the K^+ concentration varies in response to channel gating. □

Methods

Generation and sequencing of the monoclonal antibody

Monoclonal antibody (mouse immunoglobulin-γ (IgG)) against KcsA was obtained as described[23]. Total messenger RNA was isolated from the mouse hybridoma cells using TRIZOL reagents (Gibco BRL). The complementary DNA encoding the variable region of the antibody was obtained by reverse transcription and polymerase chain reaction (RT–PCR) by the 5′ RACE (rapid amplification of cDNA ends) system (Gibco BRL). The PCR products were cloned into pUC18 (Gibco BRL) and then sequenced.

Purification of a KcsA–Fab complex

KcsA was purified in the detergent decylmaltoside (DM) as previously described[2]. Thirty-five carboxy-terminal amino acids of KcsA were cleaved by chymotrypsin proteolysis. Mouse IgG was purified from mouse hybridoma cell culture supernatant using protein A affinity chromatography. Fab fragment of the antibody was obtained by papain proteolysis followed by Q-Sepharose chromatography. KcsA and Fab were mixed, and the complex obtained was purified on a Superdex 200 column equilibrated in 50 mM Tris buffer at pH 7.5, 150 mM KCl and 5 mM DM. For growing crystals in low K^+ concentration, the KcsA–Fab complex was dialysed against 50 mM Tris at pH 7.5, 2 mM KCl, 148 mM NaCl and 5 mM DM before we set up crystallization trials.

Crystal preparation

Crystals of space group *I*4 (high-K^+ structure, $a = b = 155.33$, $c = 76.27$, $\alpha = \beta = \gamma = 90°$; and low-$K^+$ structure, $a = b = 155.29$, $c = 75.74$, $\alpha = \beta = \gamma = 90°$) were grown at 20 °C by the sitting-drop method. For each drop, concentrated KcsA–Fab complex (7–15 mg ml^{-1}) was mixed with an equal volume of reservoir solution (20–25% PEG 400, 50 mM magnesium acetate, 50 mM sodium acetate, pH 5–5.6). Cryoprotection was achieved by increasing the PEG concentration in the reservoir to 40% in 2.5% increments, 2–3 steps per day. The concentration of K^+ in the drop increases during the cryoprotection process; the final K^+ concentration was estimated to be about 200 mM and 3 mM for crystals set up in 150 mM KCl and 2 mM KCl, respectively. Here we refer to the structure solved with protein purified in 150 mM KCl as the high-K^+ structure, and the structure solved with protein purified in 2 mM KCl as the low-K^+ structure. All crystals were frozen in liquid nitrogen.

Crystallographic analysis

Data were collected at station X-25 of the National Synchrotron Light Source (Brookhaven National Laboratory) and at station A1 and F1 of Cornell High Energy Synchrotron Source. The data were processed with Denzo and Scalepack[24]. Further data processing was performed with the CCP4 package[25]. We solved the structure of the KcsA–Fab complex in high K^+ by molecular replacement with AMORE using a published Fab structure (PDB code 1MLC) as the search model[9,26]. The published KcsA structure (1BL8) was then placed into the electron density[2]. The model was refined by several cycles of manual rebuilding (performed with program O)[27], followed by simulated annealing, minimization and individual B-factor refinement using CNS[28]. All measured data between the resolution limits of 40.0–2.0 Å were used for the refinement (except for a random 10% that was used for calculation of the R_f, during which bulk solvent and anisotropic temperature factor corrections were applied to the reflection data. The model contains 534 amino acids, 469 water molecules, 7 potassium ions and 2 partial lipid molecules.

The structure of the KcsA–Fab complex in 3 mM KCl (low-K^+ structure) was solved using the high-K^+ structure as a search model[26]. Refinement was carried out with cycles of simulated annealing, as above, starting at 3000 K[28]. All data between 30 and 2.3 Å were used in the refinement (except for a random 10% used to calculate R_f). The model contains 534 amino acids, 266 water molecules, 2 potassium ions, 1 sodium ion and 2 partial lipid molecules. Both refined models have good geometry with one Ramachandran outlier, which is in the Fab. Figure 1a was prepared with program O[27]; Figs 1b and 2–5 were prepared with Gl_Render[29,30].

Received 2 August; accepted 10 September 2001.

1. Hille, B. *Ionic Channels of Excitable Membranes* (Sinauer, Sunderland, 1992).
2. Doyle, D. A. *et al.* The structure of the potassium channel: molecular basis of K^+ conduction and selectivity. *Science* **280,** 69–77 (1998).
3. Morais-Cabral, J. H., Zhou, Y. & MacKinnon, R. Energetic optimization of ion conduction rate by the K^+ selectivity filter. *Nature* **414,** 37–42 (2001).
4. Armstrong, C. M. Interaction of tetraethylammonium ion derivatives with the potassium channels of giant axons. *J. Gen. Physiol.* **58,** 413–437 (1971).
5. Liu, Y., Holmgren, M., Jurman, M. E. & Yellen, G. Gated access to the pore of a voltage-dependent K^+ channel. *Neuron* **19,** 175–184 (1997).
6. Perozo, E., Cortes, D. M. & Cuello, L. G. Structural rearrangements underlying K^+-channel activation gating. *Science* **285,** 73–78 (1999).
7. Ostermeier, C., Iwata, S., Ludwig, B. & Michel, H. Fv fragment-mediated crystallization of the membrane protein bacterial cytochrome *c* oxidase. *Nature Struct. Biol.* **2,** 842–846 (1995).
8. Ostermeier, C., Harrenga, A., Ermler, U. & Michel, H. Structure at 2.7 Å resolution of the *Paracoccus denitrificans* two-subunit cytochrome *c* oxidase complexed with an antibody Fv fragment. *Proc. Natl Acad. Sci. USA* **94,** 10547–10553 (1997).
9. Braden, B. *et al.* Three-dimensional structures of the free and the antigen-complexed Fab from monoclonal anti-lysozyme antibody D44.1. *J. Mol. Biol.* **243,** 767–781 (1994).
10. Roux, B. & MacKinnon, R. The cavity and pore helices in the KcsA K^+ channel: electrostatic stabilization of monovalent cations. *Science* **285,** 100–102 (1999).
11. Otting, G., Liepinsh, E. & Wuthrich, K. Protein hydration in aqueous solution. *Science* **254,** 974–980 (1991).
12. Speakman, J. C. Acid salts of carboxylic acids, crystals with some "very short" hydrogen bonds. *Struct. Bonding (Berlin)* **12,** 141–199 (1972).
13. Dobler, v. M., Dunitz, J. D. & Kilbourn, B. T. Die struktur des KNCS-Komplexes von nonactin. *Helv. Chim. Acta* **52,** 2573–2583 (1969).
14. Neupert-Laves, K. & Dobler, M. The crystal structure of a K^+ complex of valinomycin. *Helv. Chim. Acta* **58,** 432–442 (1975).
15. Dunitz, J. D. & Dobler, M. in *Biological Aspects of Inorganic Chemistry* (eds Addison, A. W., Cullen, W. R., Dolphin, D. & James, B. R.) 113–140 (Wiley, New York, 1977).
16. Jencks, W. P. *Catalysis in Chemistry and Enzymology* (Dover, New York, 1987).
17. Swenson, R. P. Jr & Armstrong, C. M. K^+ channels close more slowly in the presence of external K^+ and Rb^+. *Nature* **291,** 427–429 (1981).
18. Miller, C., Latorre, R. & Reisin, I. Coupling of voltage-dependent gating and Ba^{2+} block in the high-conductance, Ca^{2+}-activated K^+ channel. *J. Gen. Physiol.* **90,** 427–449 (1987).
19. Demo, S. D. & Yellen, G. Ion effects on gating of the Ca^{2+}-activated K^+ channel correlate with occupancy of the pore. *Biophys. J.* **61,** 639–648 (1992).
20. Hoshi, T., Zagotta, W. N. & Aldrich, R. W. Shaker potassium channel gating. I: Transitions near the open state. *J. Gen. Physiol.* **103,** 249–278 (1994).
21. Zheng, J. & Sigworth, F. J. Intermediate conductances during deactivation of heteromultimeric Shaker potassium channels. *J. Gen. Physiol.* **112,** 457–474 (1998).
22. Lu, T. *et al.* Probing ion permeation and gating in a K^+ channel with backbone mutations in the selectivity filter. *Nature Neurosci.* **4,** 239–246 (2001).
23. Harlow, E. & Lane, D. *Antibodies: A Laboratory Manual* (Cold Spring Harbor Laboratory Press, Cold Spring Harbor, 1989).
24. Otwinowski, Z. & Minor, W. Processing of X-ray diffraction data collected in oscillation mode. *Methods Enzymol.* **276,** 307–326 (1997).
25. Collaborative Computational Project, No. 4. The CCP4 Suite: Programs for X-ray crystallography. *Acta Crystallogr. D* **50,** 760–763 (1994).
26. Navaza, J. AMoRe: an automated package for molecular replacement. *Acta Crystallogr. A* **50,** 157–163 (1994).
27. Jones, T. A., Zou, J. Y., Cowan, S. W. & Kjeldgaard, M. Improved methods for building protein models in electron density maps and the location of errors in these models. *Acta Crystallogr. A* **47,** 110–119 (1991).
28. Brunger, A. T. *et al.* Crystallography & NMR system: A new software suite for macromolecular structure determination. *Acta Crystallogr. D* **54,** 905–921 (1998).
29. Kraulis, P. MOLSCRIPT: a program to produce both detailed and schematic plots of protein structures. *J. Appl. Crystallogr.* **24,** 946–950 (1991).
30. Bacon, D. & Anderson, W. F. A fast algorithm for rendering space filling molecule pictures. *J. Mol. Graph* **6,** 219–220 (1988).

Acknowledgements

We thank the staff at the National Synchrotron Light Source X-25 and Cornell High Energy Synchrotron Source A1 and F1 for assistance, Y. Jiang for help and advice at many stages of this project, F. Weis-Garcia and M. Nussenzweig for advice and teaching monoclonal methods, R. Dutzler for lipid topology files, and F. Valiyaveetil and J. Dunitz for discussions. This project was supported by a grant from the National Institutes of Health to R.M. R.M. is an investigator in the Howard Hughes Medical Institute.

Correspondence and requests for materials should be addressed to R.M. (email: mackinn@rockvax.rockefeller.edu). Coordinates have been deposited with the Protein Data Bank under accession codes 1K4C and 1K4D.